Journal of Physics: Conference Series **708** (2016) 012013 doi:10.1088/1742-6596/708/1/012013

Coherent structures in a zero-pressure-gradient and a strongly decelerated boundary layer

Mark P Simens[1], Ayse G Gungor[2], Yvan Maciel[3]

[1] School of Aeronautics, Universidad Politécnica de Madrid, 28040 Madrid, Spain
[2] Faculty of Aeronautics and Astronautics, Istanbul Technical University, 34469 Maslak, Istanbul, Turkey
[3] Department of Mechanical Engineering, Laval University, Quebec City, QC, G1V 0A6 Canada

E-mail: ayse.gungor@itu.edu.tr

Abstract. Coherent structures in a strongly decelerated large-velocity-defect turbulent boundary layer (TBL) and a zero pressure gradient (ZPG) boundary layer are analysed by direct numerical simulation (DNS). The characteristics of the one-point velocity stastistics are also considered. The adverse pressure gradient (APG) TBL simulation is a new one carried out by the present authors. The APG TBL begins as a zero pressure gradient boundary layer, decelerates under a strong adverse pressure gradient, and separates near the end of the domain in the form of a very thin separation bubble. The one-point velocity statistics in the outer region of this large-defect boundary layer are compared to those of two other large-velocity-defect APG TBLs (one in dynamic equilibrium, the other in disequilibrium) and a mixing layer. In the upper half of the large-defect boundary layers, the velocity statistics are similar to those of the mixing layer. The dominant peaks of turbulence production and Reynolds stresses are located in the middle of the boundary layers. Three-dimensional spatial correlations of (u, u) and (u, v) show that coherence is lost in the streamwise and spanwise directions as the velocity defect increases. Near-wall streaks tend to disappear in the large-defect zone of the flow to be replaced by more disorganized u motions. Near-wall sweeps and ejections are also less numerous. In the outer region, the u structures tend to be shorter, less streaky, and more inclined with respect to the wall than in the ZPG TBL. The sweeps and ejections are generally bigger with respect to the boundary layer thickness in the large-defect boundary layer, even if the biggest structures are found in the ZPG TBL. Large sweeps and ejections that reach the wall region (wall-attached) are less streamwise elongated and they occupy less space than in the ZPG boundary layer. The distinction between wall-attached and wall-detached structures is not as pronounced in the large-defect TBL.

1. Introduction

The transposition of our knowledge acquired through the study of canonical turbulent wall flows to more complex flows such as adverse-pressure-gradient (APG) turbulent boundary layers (TBLs) is not straightforward. Consequently, a recognized and clear vision of the scaling, similarity laws and turbulence regeneration mechanisms in APG TBLs does not yet exist, which greatly impedes progress in the understanding and modeling of complex flows of this type.

For TBLs subjected to a prolonged or intense adverse pressure gradient, the layer structure and scaling parameters are known to differ from those of canonical wall flows because of their large momentum deficit and different mean strain field. Certain researchers consider that two

layers still exist, but that the nature of these layers has changed, leading to different scales (see [1]). Other researchers have proposed a three-layer structure [2, 3]. Moreover in large-defect TBLs, turbulence activity and production is small near the wall and important in the outer region of the flow [4–6]. Marquillie et al. [7] have proposed that the outer peaks of Reynolds stresses and production could be related to a streak bursting process, whereas Elsberry et al. [6] suggest that it is due to the inflectional instability of the mean velocity profile, as in mixing layers. By analysing three different large-velocity-defect TBLs, Gungor et al. [8] have concluded that these boundary layers are globally less efficient in extracting turbulent energy from the mean flow than the zero-pressure gradient (ZPG) TBL. Furthermore, it is known that the outer-region turbulent statistics of TBLs close to detachment resemble those of mixing layers [5, 8–10]. These various observations suggest that the physical mechanisms and coherent structures responsible for the production and transport of turbulence might indeed be different in APG TBLs.

Information on the coherent structures found in APG TBLs is however rare. By analyzing the direct numerical simulation (DNS) data of a turbulent separation bubble of [5], Chong et al. [11] suggested that in the APG zone prior to detachment more of the eddies which contribute to the Reynolds shear stress are eddies which are not connected to the wall. In the case of an equilibrium APG TBL, Krogstad and Skåre [12] investigated the turbulent structures with two-point space-time correlations and with quadrant analysis. The latter is based on a quadrant decomposition in the (u, v) plane, where u and v are respectively the streamwise and wall-normal fluctuating components of velocity. Intense second quadrant (Q2) motions ($u < 0, v > 0$) are usually termed ejections, while intense fourth quadrant (Q4) motions ($u > 0, v < 0$) are sweeps. These types of motions contribute significantly to the Reynolds shear stress. Krogstad and Skåre found that the lower part of the equilibrium APG boundary layer is strongly dominated by Q4 motions, while in a ZPG TBL second and fourth quadrant events are equally important. The streamwise correlation length of u was also found to be considerably shorter in the APG case throughout the boundary layer, a result also obtained later in different large-velocity-defect TBLs by [13] and [8]. Rahgozar and Maciel [14] observed that the predominance of streaky u-structures in the outer region of a large-velocity-defect TBL is less than in the ZPG case. This predominance even disappears near detachment. By analysing the same flow, Rahgozar and Maciel [13] found that large-scale u-structures are less elongated than those of ZPG TBLs, especially in the lower part of the boundary layer.

In the present work, we investigate how a strong adverse pressure gradient affects the u and uv structures through comparisons with a ZPG TBL. To achieve this goal, we analyze the three-dimensional spatial correlations of (u, u) and (u, v) and the geometric and kinematic characteristics of three-dimensional sweeps and ejections. The present study provides new information on the three-dimensional properties of sweeps and ejections found in ZPG TBLs. The properties of the one-point velocity statistics are also investigated.

2. Numerical methodology

The two direct numerical simulations used to investigate the coherent structures have been performed with the same code. The ZPG TBL was simulated by Sillero et al. [15] while the APG TBL simulation is a new one carried out by the present authors. The DNS numerical scheme is described in detail in Refs. [16] and [15]. Both flows are simulated in a parallelepiped domain over a smooth no-slip wall, with spanwise periodicity and streamwise non-periodic inflow and outflow. The Navier-Stokes equations are integrated using a fractional step method on a staggered grid, with third-order Runge-Kutta time-integration, fourth order compact spatial discretization for the convective and viscous terms, and second order discretization for the pressure in the directions perpendicular to the span, which is spectral.

The DNS database of the ZPG TBL covers the Reynolds number range $Re_\theta = 2780 - 6680$. The DNS computational setup for the present APG TBL simulation is sketched in figure 1. It

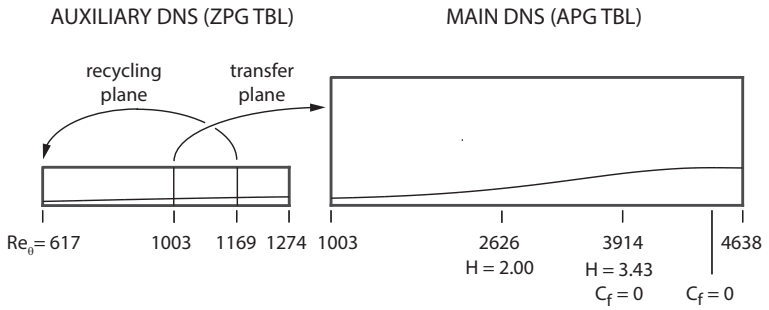

Figure 1. Schematic in the xy plane of the numerical simulation setup showing the boundary layer thickness. The computational box dimensions are to scale

consists of two simulations running concurrently [15]. The first auxiliary simulation is that of a ZPG TBL and it is intended to provide a realistic turbulent inflow for the APG layer. The inflow of the auxiliary DNS is obtained by rescaling the velocity fluctuations of a downstream plane, while fixing the inflow mean velocity to a prescribed profile [16]. The recycling plane is located at $x \approx 398\theta_0 \approx 45\delta_0$, where θ_0 and δ_0 are respectively the momentum and boundary layer thicknesses at the beginning of the auxiliary ZPG DNS. A plane located at $x \approx 268\theta_0 \approx 30\delta_0$ of the first domain is transferred at each time step into the inlet of the second main domain. The velocities at the outflow of the two computational boxes are estimated by a convective boundary condition. The outflow streamwise velocities are corrected to compensate the minimal mass flux variations due to the time-dependent inflows [16]. Table 1 summarizes the simulation parameters for both layers. For the APG DNS, the box dimensions with respect to the boundary layer thickness at the outlet are $(L_x, L_y, L_z)/\delta_{exit} = (11.0, 3.4, 2.6)$. The resolutions in terms of the Kolmogorov length η are $(\Delta x_g, \Delta y_g, \Delta z_g) < 4\eta$ except near the inlet very close to the wall where $\Delta x_g < 8\eta$. After an initial transient phase, statistics and flow fields were sampled over 53,600 time steps corresponding to a total time of $5250\theta_0/U_0$ or 10 flow throughs. A total of 134 instantaneous fields were kept, with a time interval between fields of $39.2\theta_0/U_0$.

The desired pressure gradient is controlled by imposing a streamwise dependent wall-normal velocity distribution at the upper boundary of the computational domain. The streamwise and spanwise velocities along the top boundary satisfy free-slip conditions. The imposed wall-normal velocity at the top boundary $V_{top}(x)/U_{e0}$ and the resulting streamwise velocity at the same boundary $U_{top}(x)/U_{e0}$ are illustrated in Figs. 2(a) and (b) respectively. In the design of the DNS setup, U_{top} was chosen to give an almost linear increase of the shape factor H in a central portion of the domain and to reaccelerate the flow at the end of the domain. It was obtained with boundary layer computations performed in inverse mode (H is the input, U_e is the output).

Table 1. Parameters of the APG TBL simulation. L_x, L_y, and L_z are the box dimensions along the three axes. N_x, N_y, and N_z are the collocation grid sizes. The momentum thickness θ is measured at the middle of each box.

Case	Re_θ	L_x, L_y, L_z	$(L_x, L_y, L_z)/\theta$	N_x, N_y, N_z
Auxiliary DNS (ZPG TBL)	617-1274	$88 \times 14 \times 34$	$320 \times 49 \times 126$	$1201 \times 191 \times 768$
Main DNS (APG TBL)	1003-4638	$144 \times 45 \times 34$	$118 \times 37 \times 28$	$1921 \times 380 \times 768$

3. Results and discussion

3.1. Flow description

The streamwise evolutions of U_e and of the wall-friction velocity u_τ are depicted in Fig. 2(b), where U_e is the maximum streamwise component of velocity in the wall-normal direction. The flow at the edge of the boundary layer decelerates over most of the domain but then reaccelerates at the end. As can be deduced from the evolution of u_τ, the wall shear stress decreases and eventually becomes negative. The flow separates near the exit of the domain in the form of a very thin separation bubble. The height of the zone of negative mean streamwise velocity never exceeds 0.02δ. The reacceleration of the flow at the end reattaches the boundary layer and thereby avoids encountering problems with the outflow boundary condition.

Figure 2(c) shows the streamwise evolution of three different outer pressure gradient parameters β_m, β_{zs} and β_τ, as well as the inner pressure gradient parameter $\beta_i = \nu/(\rho u_\tau^3)(dp/dx)$, often denoted p^+ in the literature. The traditional outer pressure gradient parameter, Rotta-Clauser's $\beta_\tau = -(\Delta/u_\tau)(dU_e/dx)$, assumes the outer region velocity scale to be u_τ, which is not the case for large-velocity defect TBLs such as the one considered here. β_{zs} and β_m are more appropriate outer pressure gradient parameters since they are based on velocity scales that are valid for both small and large defect TBLs. $\beta_m = -(\delta/U_m)(dU_e/dx)$ is expressed with the mixing-layer-type outer-velocity scale $U_m = 2(U_e - U(y = 0.5\delta))$ introduced by Gungor et al. [8]. $\beta_{zs} = -(\delta/U_{zs})(dU_e/dx)$ is based on the Zagarola-Smits velocity scale $U_{zs} = U_e\delta^*/\delta$. Both U_m and U_{zs} are proportional to the mean streamwise momentum deficit in the boundary layer. β_{zs} and β_m are not equivalent but their streamwise evolutions are qualitatively similar, as can be seen in Fig. 2(c).

Figure 2(c) shows that each pressure gradient parameter increases significantly in a different upstream portion of the flow. The positive gradient of these pressure gradient parameters is responsible for the increase in the streamwise mean momentum defect as shown in Fig. 2(d). β_i and β_τ tend to infinity at separation since $u_\tau = 0$. The outer pressure gradient parameters β_m and β_{zs} start decreasing in the first half of the domain. The impact of the pressure force on the outer region is therefore diminishing but this change is not strong enough to reverse the situation in terms of mean momentum defect, which keeps increasing until flow separation. The increase in momentum defect can be appreciated with the increase in the shape factor H shown in Fig. 2(d). At separation, $H = 3.43$.

3.2. One-point velocity statistics

In this section, comparisons of the one-point velocity statistics of the ZPG and large-defect TBL with other flows of interest are made. The data for the present APG flow is taken at four streamwise positions where $H = 2, 2.5, 3$ and 3.43. The fourth one is the last mesh position before separation ($C_f \approx 10^{-6}$). Besides the ZPG TBLs of [15] and [16], the other turbulent boundary layers considered are the equilibrium APG TBL of Skåre and Krogstad [4] (SK) that has a relatively large velocity defect ($H \cong 2$) and is at high Reynolds numbers ($Re_\theta = 39000$–51000) and the non-equilibrium APG TBL of Maciel et al. [17] (MRL) with increasing velocity defect that includes data at detachment ($H = 1.72$–3.85). Finally, the single-stream mixing layer of Wygnanski and Fiedler [18] (WF) is also considered because the the velocity statistics of the outer region of large-defect boundary layers closely resemble those of the high speed side of a mixing layer [5, 8–10]. The key characteristics and parameter range of the boundary layer databases are given in table 2.

Streamwise mean velocity profiles of the various flows are shown in fig. 3(a). The mean velocity defect progressively increases in the present flow. The non-equilibrium APG TBL of MRL behaves in a similar manner but only the profile at separation is shown in figure 3(a) for clarity. Excluding the wall region, the velocity profiles of the large-defect boundary layers clearly resemble the single-stream mixing layer one, with large velocity gradients, similar curvatures

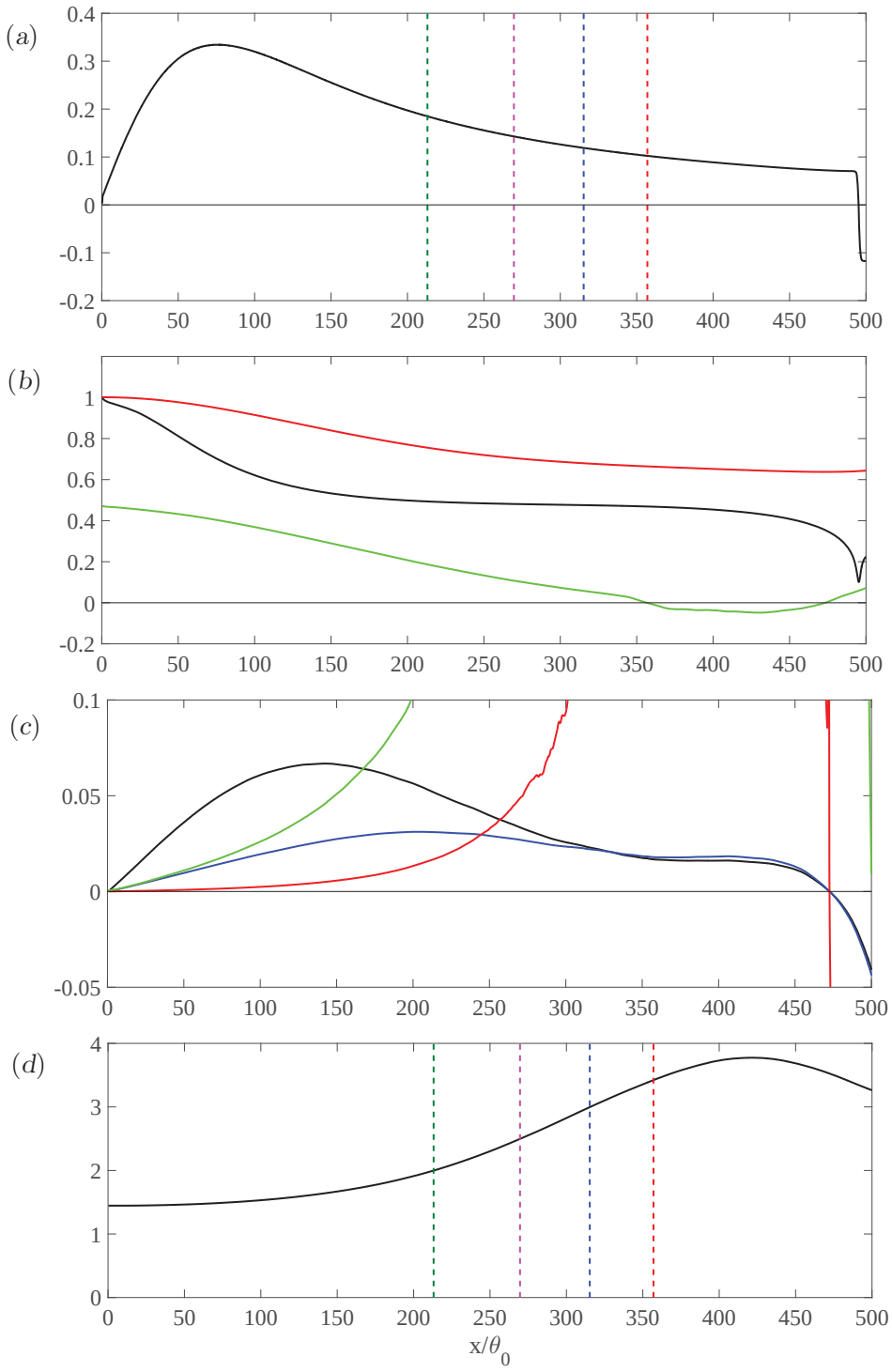

Figure 2. Mean flow parameters in the APG DNS. (a) Imposed wall-normal velocity along the top boundary. (b) Streamwise velocity at the top boundary, black; U_e/U_{e0}, red; $10u_\tau/U_{e0}$, green. (c) Pressure gradient parameters: β_m, black; β_{zs}, blue; $\beta_\tau \times 10^{-3}$, red; β_i, green. (d) Shape factor H. Vertical dashed lines in (a) and (d) denote the four streamwise positions where $H = 2$ (green), 2.5 (magenta), 3 (blue), and 3.43 (red)

Table 2. Boundary layer databases and the corresponding ranges of the parameters

Flow	Re_θ	H	β_m	β_τ
equilibrium APG TBL (SK)	39000–51000	1.99–2.01	0.092–0.094	19.6–21.4
non-equilibrium APG TBL (MRL)	3350–12691	1.72–3.85	0.099–0.043	3.2–∞
non-equilibrium APG TBL (present)	1003–4655	1.45–3.77	0–0.067	0–∞
ZPG TBL [16]	617–2139	1.41–1.54	0	0
ZPG TBL [15]	2780–6680	1.36–1.38	0	0

and the presence of an inflection point near the middle of the layer. Two of the boundary layer velocity profiles are at the same shape factor of 2, namely one for the present flow and the equilibrium one of SK, but the shapes of these profiles are very different. Since the present flow is a disequilibrium boundary layer, such a shape difference is expected. It is probably more related to the different streamwise evolution of the flows than to the dissimilarity in Reynolds number. Figure 3(a) also shows two profiles at separation, one for the present flow and one for the MRL flow. In this case, the different behaviour near the wall may be due to differences in both streamwise evolution of the TBLs and Reynolds number.

Figure 3(b) shows the mean velocity profiles normalized with the friction-viscous scales (u_τ and ν/u_τ) of the present flow, the equilibrium TBL of SK and the ZPG TBL. Profiles at separation cannot be normalized with the friction-viscous scales since in this case $u^+ \to \infty$ and $y^+ \to 0$. Even if at low Reynolds number, the ZPG TBL profile follows fairly closely the law of the wall throughout the inner region. As already shown by SK, the equilibrium APG TBL follows the logarithmic law in the overlap layer even if C_f is relatively low. This is coherent with the fact that the inner pressure gradient parameter β_i is low in this flow, $\beta_i = 0.013$, which is a

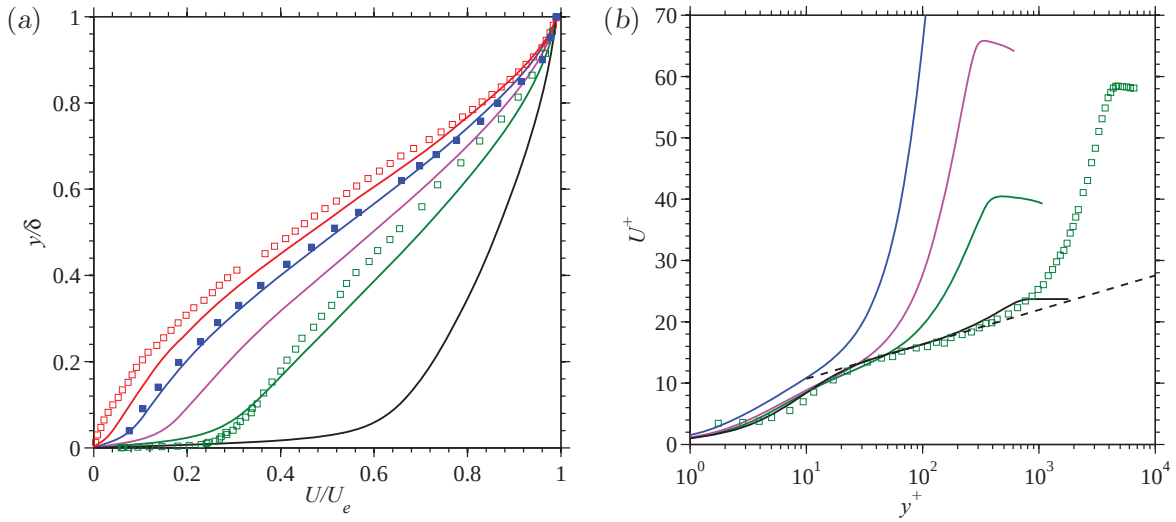

Figure 3. Mean velocity profiles normalized with (a) U_e and δ, and (b) friction-viscous scales. Present non-equilibrium APG TBL: $H = 2.0$, green line; $H = 2.5$, magenta line; $H = 3.0$, blue line; $H = 3.43, C_f = 0$, red line. ZPG TBL of [16] at $Re_\theta = 2000$, black line; equilibrium APG TBL of SK, green open square; profile at separation of the non-equilibrium APG TBL of MRL, red open square; and mixing layer of WF, blue full square. Dashed line, log law with $\kappa = 0.41$ and $B = 5.1$.

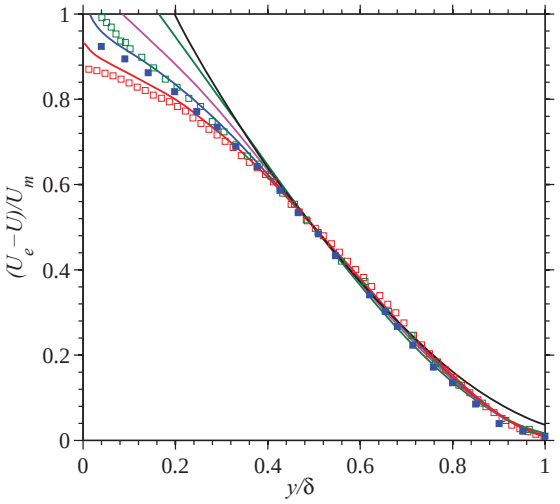

Figure 4. Velocity defect profiles normalized with U_m. Lines and symbols as in figure 3.

consequence of the high Reynolds number. The equilibrium state reached by the inner region in the SK flow, with β_i nearly constant, is therefore very similar to that of canonical wall-bounded flows. In contrast, the non-equilibrium TBL deviates from the law of the wall throughout the inner region and the departure increases as β_i increases. This confirms that the pressure force can play an important role even in the viscous sublayer in strong APG flows and that it has to be taken into account in the law of the wall [1, 19, 20]. However, as it was just mentioned, the Reynolds number also plays a role here. If the Reynolds number of the flow was higher, β_i would be lower and the departure from the law of the wall would be probably less important [21].

The velocity defect profiles of the various flows normalized with U_m are presented in fig. 4. The defect profiles are not identical, as expected, but they are all regrouped which indicates that the choice of U_m and δ as common outer scales is indeed adequate to compare velocity statistics between these flows. With the exception of the ZPG TBL, the velocity defect profiles of all other flows are actually very similar on the high-speed side, $y > 0.5\delta$. In agreement with previous studies [22, 23], U_{zs} and δ are also found to be appropriate outer scales for the mean velocity defect of all boundary layers (not shown), but U_{zs} cannot be used for the mixing layer.

The streamwise Reynolds normal stress and the Reynolds shear stress of the various flows are shown respectively in figs. 5(a) and 5(b). The Reynolds stresses are normalized with the common outer scale U_m in order to be able to compare the mixing layer and the boundary layers. For all Reynolds stresses, even $\langle v^2 \rangle$ and $\langle w^2 \rangle$ not shown, the general trend observed is one of a decrease of the stresses with increasing mean velocity defect throughout the boundary layer but especially near the wall. Since U_m is proportional to the mean strain rates present in the outer region, the fact that all the Reynolds stresses normalized with U_m decrease with velocity defect throughout the outer region implies that large-defect TBLs are less efficient in transferring energy from the mean flow to turbulence.

The behaviour of the Reynolds stresses of the TBLs subjected to a strong APG shown in figs. 5(a) and 5(b) is typical of that seen in other strongly decelerated flows. The maximum of all Reynolds stresses is in the outer region and it shifts further away from the wall with increasing velocity defect. Furthermore, the near-wall peak of $\langle u^2 \rangle$ is not present or has almost vanished.

The comparison of the three large-defect flows indicates that when the shape factor is identical or similar, the level of the various Reynolds stresses normalized with U_m is also similar. For instance, the Reynolds stress profiles at $H = 2$ from the present flow and from SK (green) differ in shape, with maxima at different locations, but are at comparable levels for all Reynolds stresses. In the case of the profiles at separation, the Reynolds stress profiles of the present

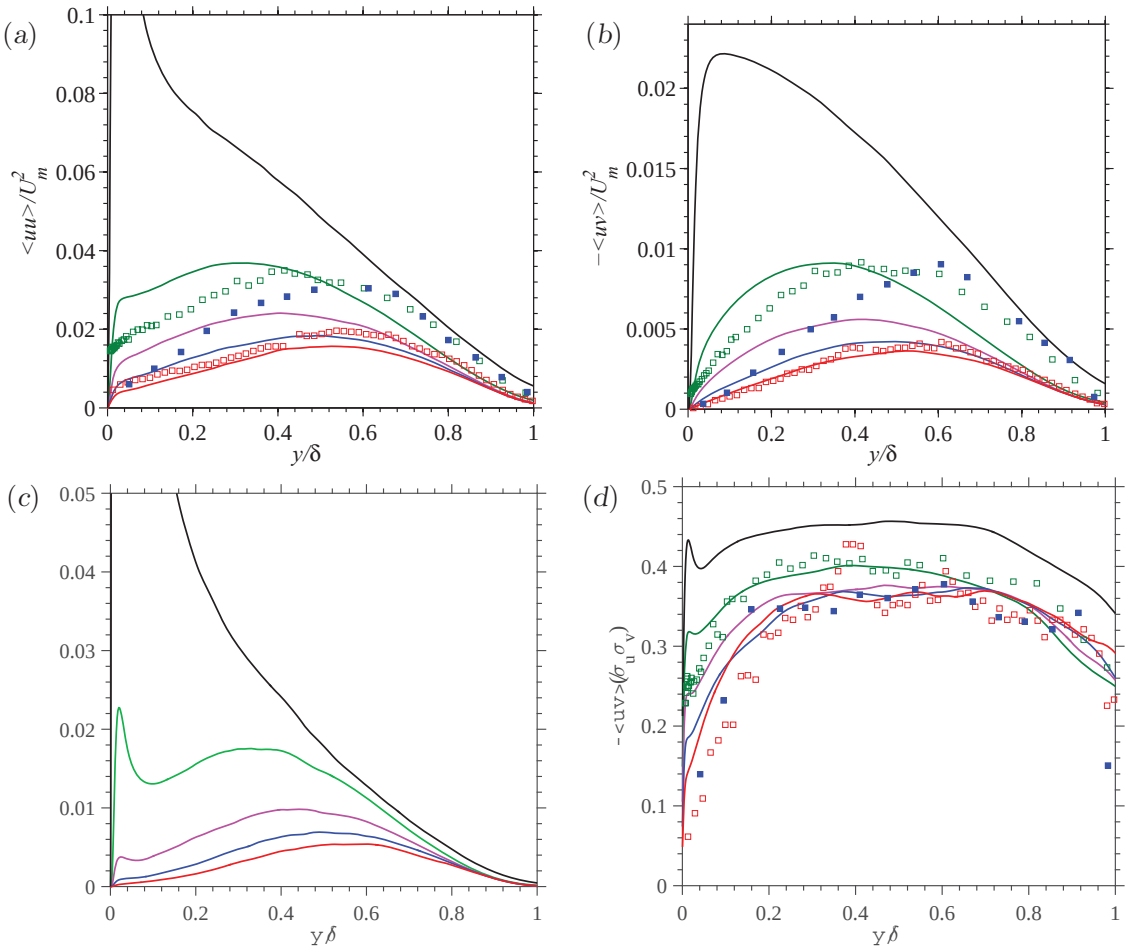

Figure 5. (a) Streamwise Reynolds normal stress and (b) Reynolds shear stress normalized with U_m. (c) Production of turbulent kinetic energy normalized with U_m and δ. (d) uv-correlation factor. Lines and symbols as in fig. 3.

flow and of the MRL flow are actually quite similar. These results suggest that the effect of the upstream history is not as important as the effect of the local mean shear, at least for these three very different large defect TBLs. Interestingly, the Reynolds stress profiles of the mixing layer are similar in shape to the profiles at separation of the boundary layers. The Reynolds stresses are however stronger in the mixing layer. Since the mean shear distribution is similar between these two types of flows (see fig. 4) the coherent structures are necessarily affected by one of the following factors or, most probably, by both of them: the presence or not of a wall and the upstream history of the flow.

The difference between ZPG and large-defect APG TBLs is even more pronounced for the production of turbulent kinetic energy as shown in fig. 5(c). As the velocity defect increases, the near-wall production peak decreases very rapidly and vanishes near separation. A production maximum appears in the outer region and its shift away from the wall follows that of the maximum of the Reynolds stresses. Figure 5(c) confirms that the present large-defect TBL is globally less efficient in extracting turbulent energy from the mean flow than the ZPG one. This has also been shown by Gungor et al. [8] for two other types of large-defect TBLs. They had also shown that the turbulent kinetic energy budget terms of the mixing layer are qualitatively

similar to those of the large-velocity-defect TBLs.

Figure 5(d) shows the uv correlation factor for the various flows, where σ_u and σ_v are respectively the local standard deviations of u and v. The level of correlation between u and v is higher in the ZPG TBL than in all other flows. In the case of the APG TBLs, the correlation of u and v is seen to deteriorate as the mean velocity defect increases, especially near the wall. Lower correlation levels for large-defect TBLs had already been noted by [24] and [8]. The correlation profiles of the mixing layer and of the APG TBL of MRL at separation are strikingly similar. They suggest that turbulence significantly looses its coherency in the low-speed side of these flows.

3.3. Two-point correlations

The spatial organization of u and uv is now investigated using three-dimensional spatial correlations. In physical space, the two-point cross-correlation coefficient for two generic variables a and b is defined as

$$C_{ab}(\vec{r},\vec{r'}) = \frac{\langle a(\vec{r})b(\vec{r'})\rangle}{\sigma_a(\vec{r})\sigma_b(\vec{r'})}, \tag{1}$$

where $\vec{r}$ is the reference position and $\vec{r'}$ the moving one. The averaging is over time and spanwise direction. The correlation functions are actually computed in Fourier space in the homogeneous spanwise direction and then Fourier transformed.

Figure 6 presents three-dimensional views of C_{uu} with the reference point at $y = 0.6\delta$ for three streamwise positions of the APG TBL corresponding to $H = 2$, 2.5 and 3.45 (separation). The three-dimensional representation of Sillero et al. [25] for their ZPG TBL at $Re_\theta = 4850$ is also included in the figure for comparison. The four plots are for a domain of size $6\delta \times 1.2\delta \times 2\delta$ in x, y and z respectively, centered at the reference point. The isosurfaces $C_{uu} = 0.09$ (turquoise) and $C_{uu} = -0.09$ (white) clearly show that the regions of positive and negative coherence of u are shorter and more inclined with respect to the wall for the large-defect TBL in comparison to a ZPG TBL. It suggests that large-scale u structures are shorter and more inclined in this large-defect TBL. The streamwise extent of the isosurface $C_{uu} = 0.09$ is about 4δ for the ZPG TBL and 2δ for the APG TBL. Moreover, both the positive and negative regions become smaller as the velocity defect increases. The negative-positive-negative spanwise trend has almost disappeared at separation. Streamwise-spanwise sections of C_{uu} at various heights in the outer region confirm that the negative C_{uu} contours are much smaller than in the ZPG TBL and they shrink in size as the velocity defect increases. In the case of the APG TBL of Rahgozar and Maciel [13], the contour $C_{uu} = -0.02$ has disappeared at separation at $y = 0.2\delta$. These results suggest that the streaky pattern of large-scale u structures occurs less frequently as the defect increases.

Streamwise-wall-normal maps of C_{vu} are shown in fig. 7 for a reference point at $y = 0.4\delta$. At that wall-normal height, the Reynolds shear stress is high in the APG TBL as shown in fig. 3(c). For the APG TBL, the low-level contours are noisy due to the insufficient number of statistically independent flow realizations. As expected, the negative value of the cross-correlation indicates that Q2 and Q4 motions are dominant. It is interesting to note that for all the cases shown in fig. 7 there is a different behaviour between the high negative level contours close to the reference point and the low negative level contours further away. The contours near the reference point are compact and inclined in the upstream direction. They reflect the character of smaller-scale intense Q2 and Q4 motions and the inclination angle is similar to what Adrian et al. [26] have observed for strong Q2 and Q4 motions in a ZPG TBL. This inclination angle is maintained as the velocity defect increases. The weak larger-scale contours are streamwise elongated in the case of the ZPG TBL and inclined in the downstream direction. They resemble the C_{uu} contours in the same plane (not shown). Sillero et al. [25] suggested that they probably reflect the combination of long u streaks with a smaller sweep or ejection motion. In the case of

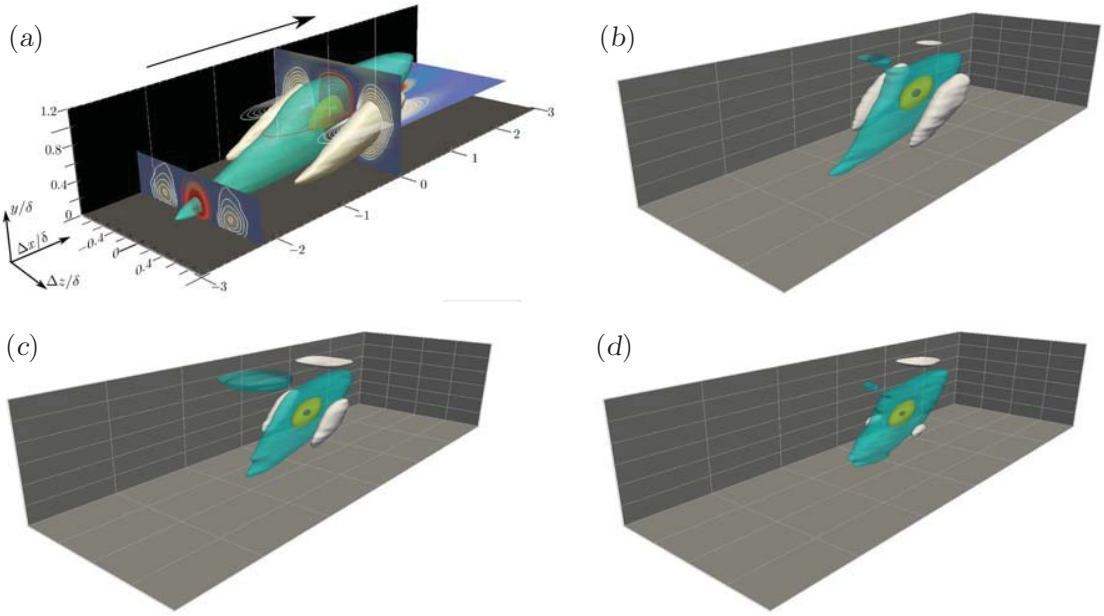

Figure 6. Three-dimensional views of C_{uu} with reference point at $y = 0.6\delta$. (a) ZPG TBL of Ref. [15] at $Re_\theta = 4850$ (fig. 1 of [25] with permission from AIP). APG TBL at positions corresponding to (b) $H = 2$ (c) $H = 2.5$ and (d) $H = 3.45$. Isosurfaces at $C_{uu} = -0.09$ (white), $+0.09$ (turquoise), $+0.4$ (yellow) and $+0.8$ (blue). Same axes ranges in all four plots

the APG TBL, the streamwise elongation of the weak large-scale contours is reduced and the inclination with respect to the wall is increased. The large-scale C_{uu} contours exhibit similar trends (not shown).

3.4. Q structures

Although they provide valuable statistical information on the structure of turbulence, two-point correlations mix the signatures of various types of coherent structures of a wide spectrum of sizes. For this reason, we now extract and directly analyze the intense three-dimensional uv structures (Qs) in both the ZPG TBL of Sillero et al. [15] and in the present APG TBL. The procedure adopted to identify the Qs follows the method used by Lozano-Durán et al. [27] (hereafter denoted LFJ). The Qs are defined as regions of connected points that satisfy simultaneously two conditions. The first condition is $|u(\vec{r})v(\vec{r})| > H^*\sigma_u\sigma_v$, where H^* is the threshold constant discussed below, also called hyperbolic-hole size. LFJ give a detailed justification of the choice of $H^*\sigma_u\sigma_v$ as the threshold function. The second condition is that all points within a Q structure are in the same quadrant of the u, v space. Point connectivity is defined with the six orthogonal neighbours. Following the notation of LFJ, the Q2 and Q4 structures will be referred to as Q^-s, and the Q1s and Q3s as Q^+s.

Table 3 presents the parameters of the subdomains used for the extraction of the Q structures. For the APG TBL, the extraction box covers the zone of large velocity defect of the flow prior to separation. The streamwise extent of the box is $5\delta_a$ where δ_a is the average boundary layer thickness inside the box. The streamwise position of the box for the ZPG TBL gives ranges of the three Reynolds numbers comparable to those of the APG TBL. $Re_m = U_m\delta/\nu$ and $Re_{zs} = U_{zs}\delta/\nu$ are Reynolds numbers of the outer region. Both extraction boxes cover the full width of the simulation domain. The same wall-normal height of $2\delta_a$ was chosen for both

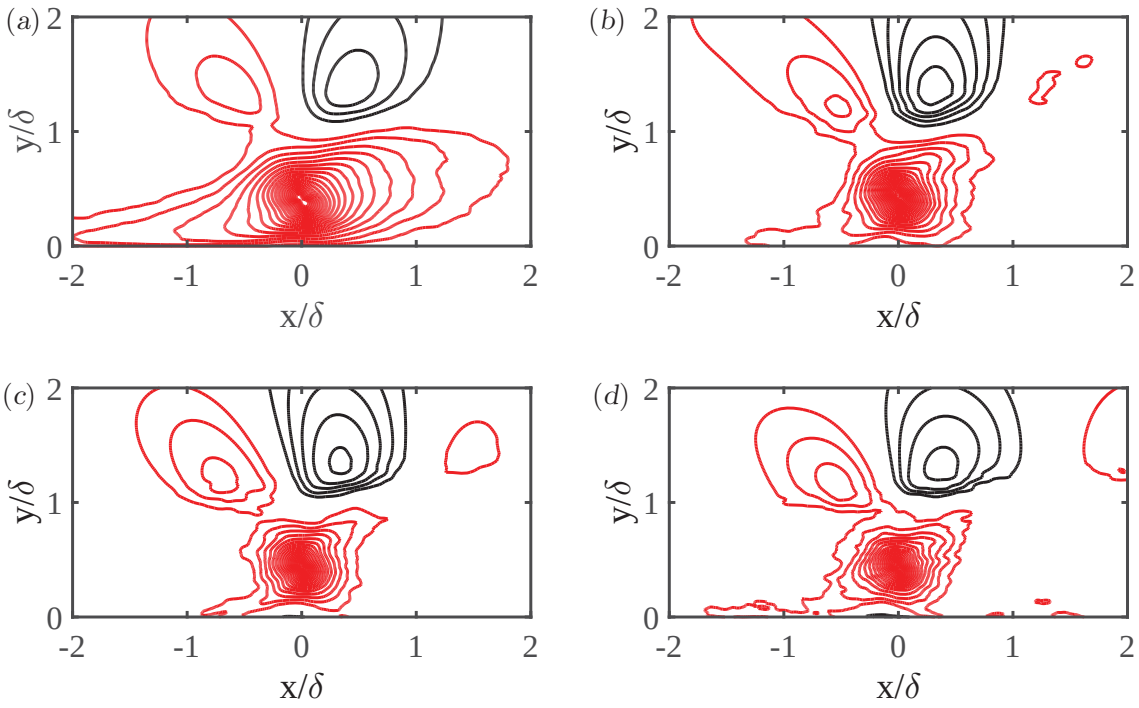

Figure 7. Streamwise-wall-normal maps of C_{vu} with reference point at $y = 0.4\delta$. (a) ZPG TBL of Ref. [15] at $Re_\theta = 4850$. APG TBL at positions corresponding to (b) $H = 2$ (c) $H = 2.5$ and (d) $H = 3.45$. Positive contours (black) start at 0.03 by increments of 0.02. Negative contours (red) start at -0.03 by increments of -0.02

boxes in order to be able to compare the volume occupied by the Qs in the two flows. Since the extraction of the Qs is computationally intensive, the number of instantaneous fields processed is limited to 27 for the ZPG TBL (box of 2.2×10^9 grid points) and 45 for the APG TBL (box of 1.7×10^8 grid points).

As in LFJ a percolation analysis has been performed to determine a value for H^* that gives an equilibrium between detecting only a few very big objects and detecting only a few small and very intense Qs. The percolation crisis (rapid change of the normalized maximum volume of the Qs while varying H^*) takes place in the range $1.2 \leq H^* \leq 2.5$. A hyperbolic hole size of $H^* = 1.75$ is chosen because it is in the middle of this range and it maximizes the number of Q^-s. It is the same value as used by LFJ in turbulent channel flows.

The linear dimensions of the Qs are defined with a rectangular box circumscribing them, the sides of this box being denoted as Δx, Δy and Δz and the midheight position of the box y_c. Structures that are as long as the streamwise length of the extraction box, $\Delta x = B_x$, are

Table 3. Parameters of the Q extraction zones. B_x, B_y and B_z are the box dimensions along the three axes and δ_a is the average boundary layer thickness inside the box. N_f is the number of flow fields used

Flow	Re_θ	Re_m	Re_{zs}	H	$(B_x, B_y, B_z)/\delta_a$	N_f
ZPG TBL	4544-5801	10195-10811	6251-6599	1.38-1.37	4.51, 2.00, 10.57	27
APG TBL	2577-3916	9204-27889	5084-13413	1.97-3.42	4.99, 2.00, 4.09	45

disregarded because the length of these structures is undetermined. Similarly, very small Qs with a volume $V < (3\Delta x_g)^3$ are rejected because their sizes are not well resolved on the numerical grid.

With the present extraction procedure, a total of 184576 Qs are identified in the APG TBL and 441217 Qs in the ZPG TBL. The difference in number corresponds approximately to the difference in volume of the extraction boxes. As LFJ found in turbulent channel flows, Q^+s are less frequent than Q^-s in both TBLs, and they occupy a much smaller fraction of the space, less than 1% of the box volume against 4 to 5% for Q^-s. Q^- structures represent 57% and 52% of all Qs in the ZPG and APG TBL respectively. Table 4 summarizes the number and volume proportions for the Q^-s. Although the number fraction of ejections and sweeps is higher in the ZPG TBL than in the large-defect TBL, the volume occupied by these structures is smaller (4.2% of the box volume against 5.3%). The reason lies in the different wall-normal distribution of these sweep and ejection motions in the two flows. In the ZPG TBL, 43% of all Q^-s are small near-wall structures (near-wall Qs are defined here as structures whose center is below 0.05δ) which is consistent with the fact that the mean shear is the strongest there [28]. In the large defect APG TBL, who has a very different mean shear distribution, only 10% of all ejections and sweeps are small near-wall structures.

Figure 8 shows the joint probability density function (pdf) of the minimum and maximum wall distances for the ejections and sweeps. The structures separate into two groups: structures reaching the wall region (wall-attached) and not reaching it (wall-detached). In both flows, the wall-attached Q^-s form the narrow vertical band of the joint pdf with $y_{min} < 0.05\delta$, while wall-detached structures form the wide diagonal band. Note that the name *wall-attached* can be misleading as it seems to imply that the structure remains attached to the wall during its whole life, which is usually not the case. In turbulent channel flows, Lozano-Durán et al. [28] have shown that wall-attached ejections are generally born with their base near the wall, but remain attached only for approximately 2/3 of their lives. Attached sweeps are the mirror image of attached ejections. They usually start as detached structures but become attached at about 1/3 of their lives and remain so thereafter.

It is seen from fig. 8 that the height of Q^-s can exceed the boundary layer thickness. Wall-attached Q^-s almost as tall as 2δ are found in both flows. In the present APG flow the probabilities are higher everywhere, except near the origin. This implies that, as was discussed above, there are definitely less small Q^-s close to the wall, in proportion, in the APG TBL than in the ZPG TBL. For the detached Q^-s (diagonal band), the contours are wider in the vertical direction for the APG TBL, which indicates that the detached structures are generally taller in that flow. They are in fact bigger in all directions as it will be confirmed below.

Wall-attached Q2s and Q4s represent 35% of the total number of Q^-s and 58% of their volume (see Table 4). In the ZPG TBL, these percentages are respectively 51% and 73%. The number and size proportions of attached ejections and sweeps are therefore considerably reduced in a

Table 4. Number and volume proportions of the Q^-s (Q2s and Q4s)

Case	ZPG TBL	APG TBL
All Q^-s	57% of all Qs 4.2% of box volume	52% of all Qs 5.3% of box volume
Near-wall Q^-s ($y_c < 0.05\delta$)	43% of all Q^-s 2% of total volume of Q^-s	10% of all Q^-s 1% of total volume of Q^-s
Wall-attached Q^-s ($y_{min} < 0.05\delta$)	51% of all Q^-s 73% of total volume of Q^-s	35% of all Q^-s 58% of total volume of Q^-s

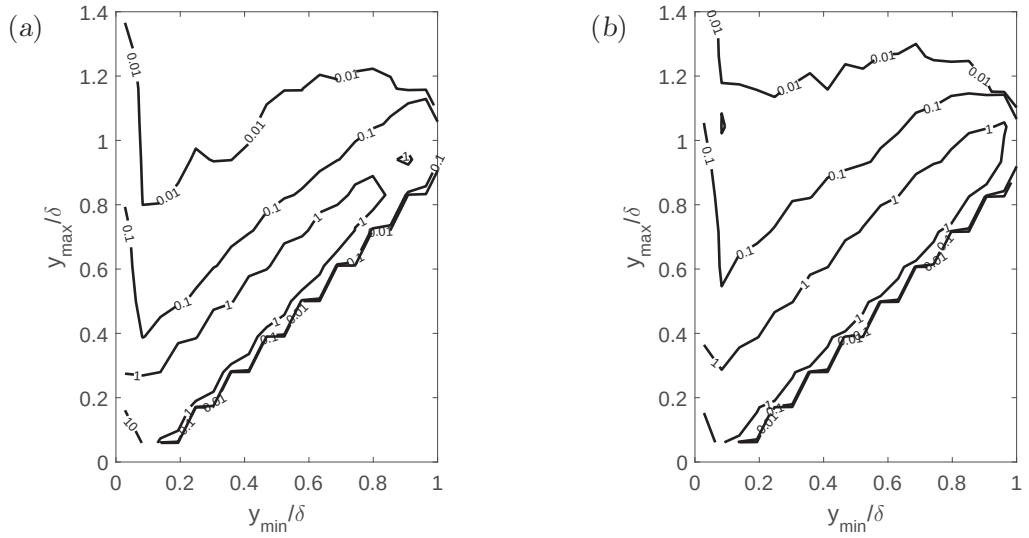

Figure 8. Joint pdf of y_{min}/δ and y_{max}/δ for Q$^-$s. (a) ZPG TBL, (b) APG TBL. Contour levels are 0.01, 0.1, 1 and 10

large-velocity-defect boundary layer. This is consistent with the fact that the turbulent activity is very small near the wall.

Figures 9 and 10 presents joint pdfs of the logarithms of the streamwise and wall-normal sizes, normalized with δ, of the boxes circumscribing Q2s and Q4s for attached and detached structures respectively. As in LFJ for turbulent channel flows, the Q2 and the Q4 structures have similar sizes, with Q2s slightly bigger. The very small attached Q4s seen in the ZPG TBL (fig. 9) are streaky sweeps flattened against the wall [28]. They do not exist in the APG TBL.

The Q$^-$s in the APG TBL are generally bigger in all directions. But the largest structures are found in the ZPG TBL with attached Q2s that can reach the length of the extraction box $\Delta_x \approx 5\delta$ while being 3 times longer than they are tall and wide. For channel flows, LFJ found very long attached Q2s reaching $\Delta_x \approx 20h$ and $\Delta_y \approx \Delta_z \approx 2h$. The rapid streamwise variations and strong non-equilibrium state of the present APG TBL probably prohibit the existence of such long motions. In this flow, the longest attached Q2s rarely exceed a length of 3δ.

In the ZPG TBL, the detached Q$^-$s are globally smaller than their attached counterparts. LFJ observed that in turbulent channel flows, detached Q$^-$s and Q$^+$s are often background fluctuations of small size, of the order of a few Kolmogorov lengths, whose contributions to the Reynolds shear stress almost cancel. In the APG TBL, the situation is very different. The size distributions of the detached Q$^-$s are not significantly different from those of the attached Q$^-$s.

In terms of aspect ratio, fig. 9 shows that the attached structures tend to be streamwise elongated but much more so for the ZPG TBL with a linear law $\Delta_x \approx 3\Delta_y \approx 3\Delta_z$ identical to the law found by LFJ in channel flows. In the APG TBL, the law is $\Delta_x \approx 1.5\Delta_y \approx 1.5\Delta_z$. In both flows, the detached structures tend to be only slightly longer than they are tall and wide with $\Delta_x \approx 1.2\Delta_y \approx 1.2\Delta_z$.

4. Conclusion

The effects of strong adverse pressure gradients on the u and uv structures, as well as on the one-point velocity statistics of TBLs have been investigated using a newly simulated APG TBL. The DNS was designed to produce a flow with an important streamwise increase of the inner and outer pressure gradient parameters leading eventually to separation in the form a very thin

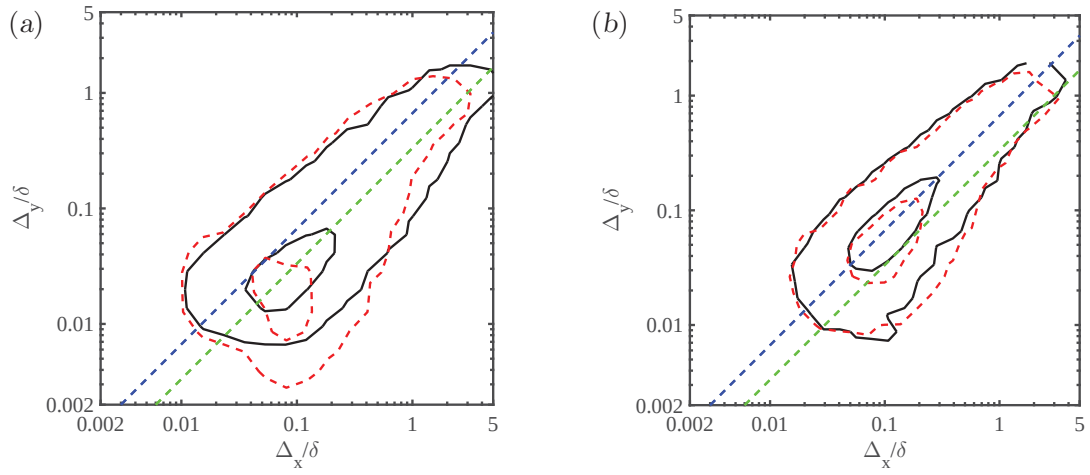

Figure 9. Joint pdfs $p(\Delta_x/\delta, \Delta_y/\delta)$ of the logarithms of the sizes of the boxes circumscribing wall-attached Q2s (black) and Q4s (red): (a) ZPG TBL, (b) APG TBL. The straight dashed lines are $\Delta_x = 1.5\Delta_y$ (blue) and $\Delta_x = 3.0\Delta_y$ (green)

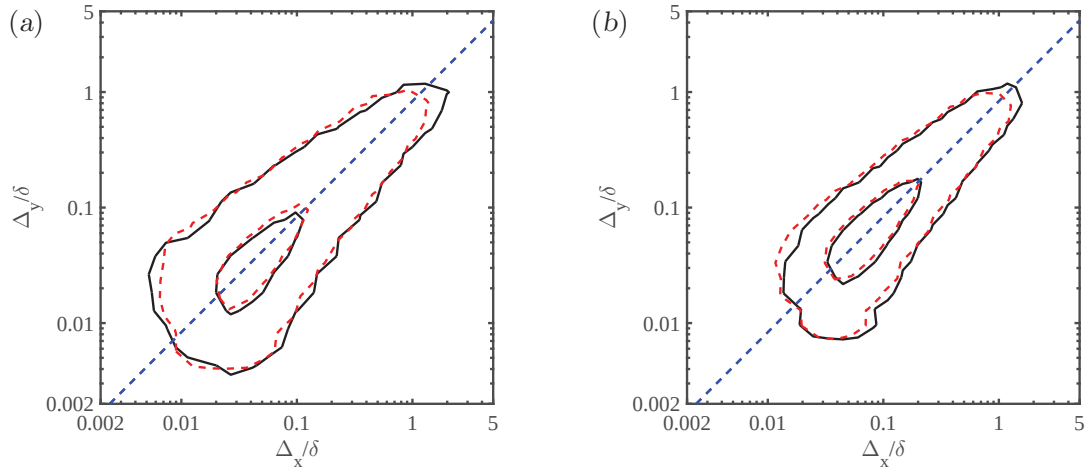

Figure 10. Joint pdfs $p(\Delta_x/\delta, \Delta_y/\delta)$ of the logarithms of the sizes of the boxes circumscribing wall-detached Q2s (black) and Q4s (red): (a) ZPG TBL, (b) APG TBL. The straight dashed blue lines are $\Delta_x = 1.2\Delta_y$

separation bubble. The sweeps and ejections found in the ZPG TBL of Sillero et al. [15] are also extracted and analyzed in order to establish a basis of comparison.

In terms of the one-point velocity statistics, the present study confirms behaviours of large-velocity-defect TBLs found in other studies. The present large-defect non-equilibrium APG TBL does not follow the classical law of the wall, even very close to the wall. In the case of both equilibrium and disequilibrium large-defect TBLs, the maximum turbulence activity is found to be in the middle of the boundary layer and not near the wall. The near-wall peak of streamwise Reynolds normal stress is absent or very small and that of turbulence production is rapidly decaying in the streamwise direction. These findings are consistent with the fact that near-wall streaks tend to disappear in the large-defect zone of the flow and are replaced by more

disorganized u motions. Near-wall sweeps and ejections are also much less numerous in the large-defect TBL in comparison to the ZPG TBL.

In the outer region of the large-defect TBL, the u structures tend to be shorter, less streaky, and more inclined with respect to the wall than in the ZPG TBL. Moreover, the two-point correlations suggest that near separation, the occurrence of side-by-side low- and high-speed structures is considerably reduced. The sweeps and ejections are generally bigger with respect to the boundary layer thickness in the large-defect boundary layer, even if the biggest structures are found in the ZPG TBL. Contrary to the ZPG TBL, wall-attached and wall-detached Q structures have similar size distributions and occupy a similar space in the boundary layer. In both flows, the attached sweeps and ejections are more streamwise elongated than their detached counterparts but the difference in aspect ratio is much less for the APG TBL.

Acknowledgments

The authors would like to thank Prof. Jiménez for organizing the First and Second Multiflow Summer Workshops. Funded in part by the Multiflow program of the European Research Council. AGG and YM were supported in part respectively by ITU-BAP and NSERC of Canada. YM thanks TUBITAK (2221 Program) for support during the collaboration stay in Turkey. The computations were made possible by generous grants of computer time from Barcelona supercomputing center and from the national center for high performance computing of Turkey. The authors would like to thank Juan Sillero and Prof. Jiménez for providing their ZPG TBL data and the programs for the two-point correlations, and Adrián Lozano-Durán and Prof. Jiménez for the processing programs for the Q structures analysis.

References

[1] Skote M and Henningson D S 2002 *J. Fluid Mech.* **471** 107–136
[2] Melnik R E 1989 *Comput. Fluids* **17** 165–184
[3] Durbin P A and Belcher S E 1992 *J. Fluid Mech.* **238** 699–722
[4] Skåre P E and Krogstad P Å 1994 *J. Fluid Mech.* **272** 319–348
[5] Na Y and Moin P 1998 *J. Fluid Mech.* **374** 379–405
[6] Elsberry K Loeffler F, Zhou M and Wygnanski I 2000 *J. Fluid Mech.* **423** 227–261
[7] Marquillie M, Ehrenstein U and Laval J P 2011 *J. Fluid Mech.* **681** 205–240
[8] Gungor A G, Maciel Y, Simens M P and Soria J 2014 *J. Phys.: Conf. Ser.* **506** 012007
[9] Simpson R L, Strickland J and Barr P 1977 *J. Fluid Mech.* **79** 553–594
[10] Driver D M 1991 *AIAA 22nd Fluid Dyn., Plasma Dyn., Lasers Conf., Honolulu, HI* (AIAA)
[11] Chong M S, Soria J, Perry A E, Chacin J, Cantwell B J and Na Y 1998 *J. Fluid Mech.* **357** 225–247
[12] Krogstad P Å and Skåre P E 1995 *Phys. Fluids* **7** 2014–2024
[13] Rahgozar S and Maciel Y 2012 *J. Turbul.* **13** 1–24
[14] Rahgozar S and Maciel Y 2011 *Exp. Therm. Fluid Sci.* **35** 15751587
[15] Sillero J, Jiménez J and Moser R 2013 *Phys. Fluids* **25** 105102–1–16
[16] Simens M, Jiménez J, Hoyas S and Mizuno Y 2009 *J. Comput. Phys.* **228** 4218–4231
[17] Maciel Y, Rossignol K S and Lemay J 2006 *Exp. Fluids* **41** 573–590
[18] Wygnanski I and Fiedler H E 1970 *J. Fluid Mech.* **41** 327–361
[19] Stratford B S 1959 *J. Fluid Mech.* **5** 1–16
[20] Mellor G L and Gibson D M 1966 *J. Fluid Mech.* **24** 225–253
[21] Nickels T B 2004 *J. Fluid Mech.* **521** 217–239
[22] Maciel Y, Rossignol K S and Lemay J 2006 *AIAA J.* **44** 2450–2464
[23] Logdberg O, Angele K and Alfredsson P H 2008 *Phys. Fluids* **20** 075104
[24] Simpson R, Chew Y T and Shivaprasad B 1981 *J. Fluid Mech.* **113** 23–51
[25] Sillero J A, Jimnez J and Moser R D 2014 *Phys. Fluids* **26** 105109
[26] Adrian R J, Meinhart C D and Tomkins C D 2000 *J. Fluid Mech.* **422** 1–54
[27] Lozano-Durán A, Flores O and Jiménez J 2012 *J. Fluid Mech.* **694** 100–130
[28] Lozano-Durán A and Jiménez J 2014 *J. Fluid Mech.* **759** 432–471